ELSEVIER

Ceramics International 26 (2000) 39–45

CERAMICS INTERNATIONAL

A study on the mechanical, abrasion and microstructural properties of zirconia-flyash material

L.N. Satapathy

Ceramic Technological Institute, Bharat Heavy Electricals Limited (BHEL), Electroporcelains Division, P.B. No. 1245, Bangalore 560 012, India

Received 22 July 1998; received in revised form 3 August 1998; accepted 2 December 1998

Abstract

The addition of zirconia in different proportions to one type of Indian flyash has been studied. The study is concentrated on mechanical properties of the materials like MOR, MOE and hardness, the sand abrasion resistance and the microstructural investigation by scanning electron microscope. It is observed that MOR of the material increases upto 10 vol% of ZrO_2 in flyash and then starts decreasing. On the other hand, both MOE and the Vickers hardness increase with the increase in ZrO_2 content in the matrix. The abrasion volume loss of the material decreases upto 15 vol% ZrO_2 in flyash which further increase with increase in ZrO_2 content. It has been pointed out from the microstructural investigation that, with the increase in addition of ZrO_2 in flyash, the needle shaped mullite phases are being replaced by the near spherical shaped zircon grains. This paper correlates these data along with the physical properties and phase identification studies, which were reported earlier.

Keywords: B. Microstructure-final; C. Mechanical properties; Abrasion; Zirconia-flyash

1. Introduction

Flyash is a by product of thermal power stations. Flyash generation, which poses a serious threat to health by air pollution is set to touch the 100 million tones per year mark by the turn of the century from the current level of 80 million tones per year in India. Flyash is a finely divided residue with particle size varying from 0.5 to 100 μm. It is refractory and abrasive in nature. Although the generation of flyash is very high in India, the utilization is only 6%, posing a serious threat to the environment.

The chemical composition of flyash is not constant due to the nature of coal available from different places. However, the main constituents of fly ash are Silica and Alumina. Many efforts in the safe disposal of the flyash waste have been made. The emphasis has been given to make value added products from flyash. Some of these products are, bricks, cement, concrete block, vibrated paving slabs, tiles, concrete making etc. A detailed review has been compiled elsewhere [1]. Efforts are also being made to develop value added ceramic materials using flyash as a raw material [2–5].

Zirconia is a versatile material and finds wide application in structural ceramics and electronic ceramic products [6–9]. The science and technology of zirconia ceramics is continuing to evolve at a considerable pace. The materials property improvements and addition with other ceramic materials for better performance, are leading to increasing applications in many industrial sectors.

An attempt has been made here to study the properties of zirconia flyash material. The physical properties, thermal expansion property and the phase identification studies for this material have been reported in this journal earlier [3]. As has been described, the zirconia reacts with silica of flyash and forms zircon ($ZrSiO_4$) as the major phase. This is in contrast to the well-studied ZrO_2–Al_2O_3 system, where, ZrO_2 does not react with alumina at the sintering temperature [10]. In this work, the study on the mechanical properties of the material like three point bend strength (MOR), Modulus of Elasticity (MOE), Vickers hardness, the sand abrasion resistance test have been carried out. The major emphasis has been given to study the variation in microstructure of the material with varying ZrO_2 content. A correlation of the properties has been established.

2. Experimental

The Flyash used in this experiment was obtained from Raichur thermal power station, Karnataka, India.

0272-8842/99/$20.00
PII: S0272-8842(99)00017-6

The chemical composition of the powder is given in Table 1. The average particle size (D50) value of this material was found to be 3.76 μm and with a specific gravity of 2.4. A high purity grade 3 mol% yttria stabilized zirconia, prepared at our laboratory was used in this study. The powder had an average particle size of < 0.5 μm.

Stoichiometric compositions of zirconia were added in flyash. Different batches having 0, 5, 10, 15, 20 and 25% of zirconia in flyash were dispersed in alcohol medium with a suitable dispersant. Each mixture was pulverized separately in a Fritsch pulverisette for 8 h using alumina bowls and alumina balls. The slurry was mixed with 2 wt% polyethylene glycol (PEG - 4000) binder in solution form and again pulverized for 1 h. Then the mixture was dried to get back the powder and was sieved to form soft granules. These granules were used for compaction. The batches were named as F-0, F-5, F-10, F-15, F-20 and F-25 for the samples containing 0, 5, 10, 15, 20 and 25% zirconia in flyash matrix respectively.

The granulated powders were uniaxially pressed at different pressure to make bars for MOR and abrasion resistance tests. Rectangular bars of approximate green dimension $60\times6\times5$ mm^3 were fabricated at 345 kg/cm^2 pressure, for three point bend strength test. Also, rectangular bars of approximate green dimension $80\times27\times7$ mm^3 were fabricated at 101 kg/cm^2 for sand abrasion test.

The samples were dried at 110°C for 12 h prior to firing in an open tunnel kiln at 1255 ± 5°C. The fired samples were used for characterization studies. 5×5 mm^2 samples were diamond cut from the sintered MOR bars and polished with emery paper ranging from 200 to 800 grit mesh size. Then, these samples were polished with diamond paste in a Struers DAP-7 automatic polisher down to 1 μm level. The samples were etched in 10% hydrofluoric acid (HF) solution for 20 s. These samples were gold coated prior to the investigation under a scanning electron microscope (SEM, JEOL 5200 model). After the SEM test, these samples were used for Vickers microhardness measurement with a diamond square based pyramid indenter using HSV-20 Shimadzu model hardness tester at 1 kg load. The three point bend strength measurement was carried out using Lloyds Universal testing machine, following ASTM standard. The modulus of elasticity was measured by resonant frequency method on rectangular samples using ASTM C 623-92 standard. The sand abrasion test of the sample was carried out using ASTM G 65 standard on an indigenous machine.

Table 1
Chemical composition of flyash used in this work

Sl.No	Chemical name	Chemical composition	Wt%
1	Silica	(SiO_2)	57.00
2	Alumina	(Al_2O_3)	29.00
3	Iron oxide	(Fe_2O_3)	06.50
4	Calcium oxide	(CaO)	03.90
5	Magnesium oxide	(MgO)	01.10
6	Potassium oxide	(K_2O)	00.30
7	Sodium oxide	(Na_2O)	00.21
8	Titanium dioxide	(TiO_2)	00.13
9	Loss on Ignition	(LOI)	1.86

3. Results and discussion

The physical properties like green density, bulk density, % apparent porosity (% AP) and thermal expansion coefficients and the phase identification studies for these materials have been published in this journal [3]. This paper will describe the mechanical properties like modulus of rupture (MOR), modulus of elasticity (MOE), Vickers hardness and the abrasion volume loss from the sand abrasion test and finally the microstructural investigation of this series of material. Table 2 summarizes the above results.

The bulk density tended to increase with the increase of addition of zirconia. This is because, with the addition of ZrO_2 in the matrix, more and more zircon ($ZrSiO_4$) is being formed [3], which signifies the rise in density.

The three point bend strength data (Fig. 1) showed an increasing trend with the addition of zirconia up to 10

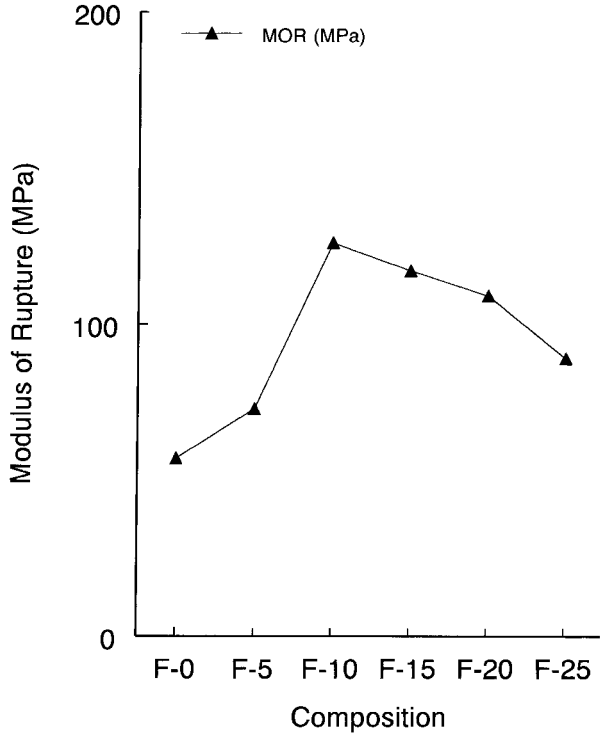

Fig. 1. Variation of modulus of rupture of flyash with zirconia addition —▲— MOR (MPa).

wt%. Further addition into the flyash matrix reduces the three point bend strength of the material.

This can be explained on the basis that, with the addition of ZrO_2 into the flyash matrix, the part of the glassy phase is being substituted by the particle shaped zircon phase. The fibrous structure of the mullite phase provides the reinforcement in the structure resulting from the increase in strength. Probably 10–15% of ZrO_2 is ideal in the flyash matrix to provide a balance of particle like $ZrSiO_4$ phase and the needle like mullite phase to provide higher strength. As the $ZrSiO_4$ phases dominate at higher ZrO_2 content in flyash, the effect of reinforcement reduces resulting in reduction of strength. As can be seen in the Fig. 1, there is a drastic jump in MOR from F-5 to F-10 composition, which marginally drops at F-15. The reduction in MOR becomes more prominent at the higher ZrO_2 content in the matrix.

The modulus of elasticity (MOE) of these materials as measured by the resonant frequency method revealed an increasing trend with the addition of ZrO_2 into the matrix (Fig. 2). By closely looking at the result, it was observed that, the MOE values follow an almost linear increase in data confirming the applicability of rules of mixture. It is known that, the elastic modulus of material depend on phase constitution and the shape and distribution of any porosity. With the increase in ZrO_2 addition, the high modulus Zircon ($E \approx 140 - 160$ GPa) is being more prominent compared to the low modulus mullite ($E \approx 100 - 140$ GPa) phase, which increases the modulus of elasticity of the material.

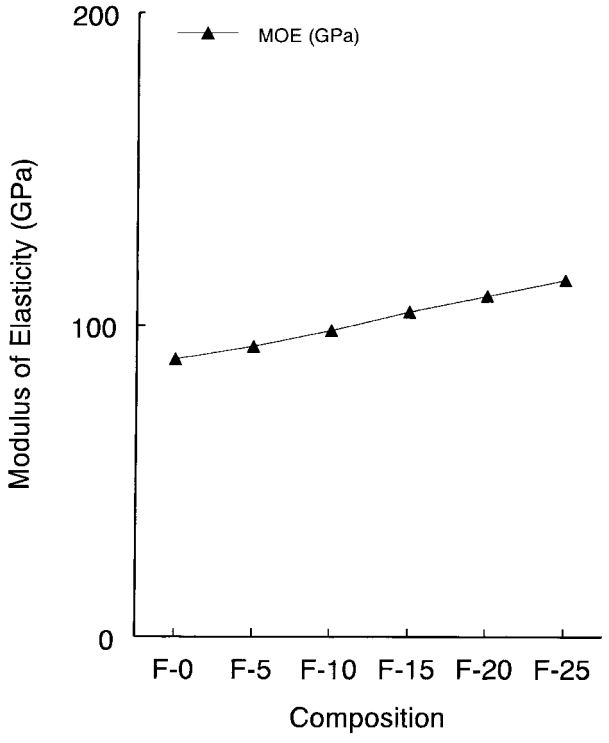

Fig. 2. Variation of modulus of elasticity of flyash with zirconia addition —▲— MOE (GPa).

Also, all elastic properties are influenced by the level of porosity since pores act as a second phase of a zero modulus. The porosity reduces Young's modulus according to the relationship of the form [15].

$$E = E_0 \exp(-av)$$

where

E_0 = modulus of dense material
v = volume fraction of porosity
a = constant determined by Poisson's ratio and also by pore shape and distribution.

However, as reported earlier [3], these materials are fully dense except F-10 and F-15 composition which showed a marginal 0.3% apparent porosity. But, this amount really did not reflect in the reduction of MOE in these two samples. Hence, the phase composition alone plays an important role in the observed MOE behaviour of the materials.

The Vickers hardness measurement was carried out on a diamond square based pyramid indenter using 1 kg load. The Vickers microhardness is calculated using the formula.

$$HV = 1.8544\ P/d^2,$$

where P = load, d = mean diameter of the indent

The hardness data have been expressed as $XHV1.0$, where, X is the hardness value. As Fig. 3 suggests, the hardness value of these materials increased with the increase in ZrO_2 content in the matrix. This may be due to the fact that a higher hardness material like Zircon increases the hardness of the new material. It is also observed that, the increase in hardness was following a regular trend. However, the scatter in data was found to be high, although the coefficient of variation (CV) value remained within the 12% range which is the well accepted value for microhardness data in the load range of 10–1000 g.

The scatter in hardness data in ceramics occur due to

1. their multiphase nature;
2. their generally non-cubic crystal symmetry;
3. the porosity which may be seen below the surface of the test piece.

All these factors are effective in the class of ceramics under study here. These factors can exert some influence over the local response of the indenter leading to variation in the hardness data. However, if the data lie within the permissible limit of the coefficient of variation value, then it is accepted.

The adjusted abrasion volume loss of the material measured by the sand abrasion test revealed a decreasing

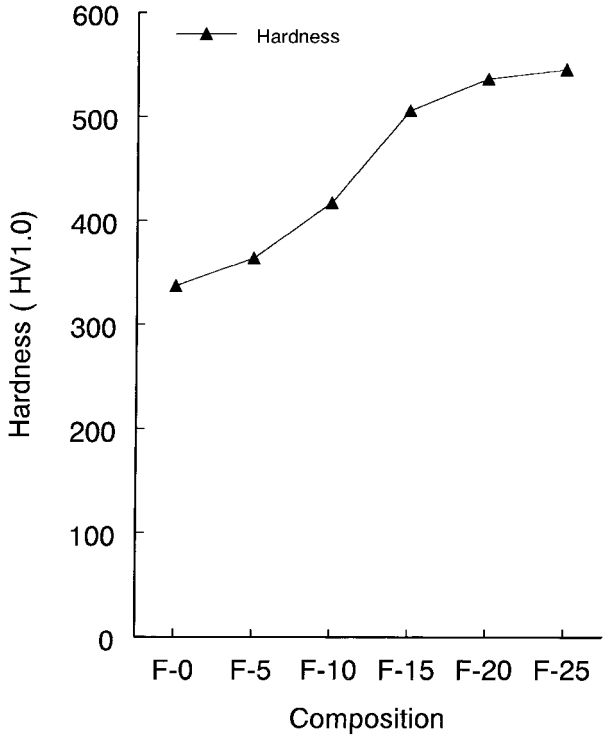

Fig. 3. Variation of Vicker's hardness of flyash with zirconia addition —▲— hardness.

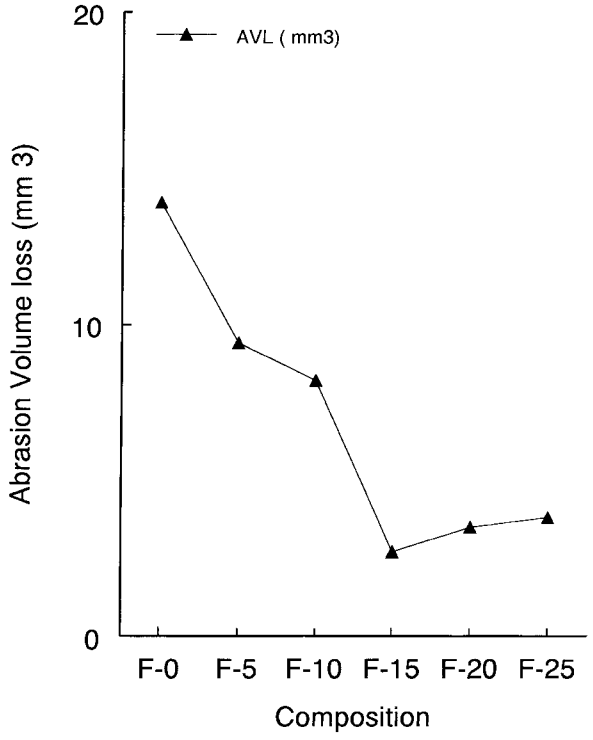

Fig. 4. Variation of abrasion volume loss of flyash with zirconia addition —▲— AVL (mm^3).

trend upto F-15 composition, after which there was marginal increase in value (Fig. 4). The volume loss is calculated as follows:

$$\text{measured volume loss } (MVL) = \left[\{\text{mass loss (g)/density (g/cc)}\}^{*}1000\right]\text{mm}^3$$

The data are represented as adjusted volume loss in mm^3, taking into account the abrasion of the rubber wheel during the test following the formula:

$$\text{adjusted volume loss} = \left[\text{MVL}^{*}\{228.6\text{ mm/diameter of the wheel(mm) after test}\}\right]$$

In many cases, the abrasion volume loss is a function of hardness, strength, MOE and porosity of the material. On a closer look at Table 2, it was observed that, the hardness and MOE values were increased throughout, MOR increased upto F-10 composition and the apparent porosity does not have much of a role here, since, all the samples had almost having no open porosity. As a result of all the above, the volume loss of the material was expected to be highest for pure flyash and should decrease with the addition of ZrO_2 in matrix. The observed result followed this trend. However, there was a marginal increase in the volume loss of the material in the F-20 and F-25 compositions. This behaviour has probably originated from the lower strength of these materials due to the less interlinkage of the grains. It is to be noted here that, the AVL value for the F-15 composition is very low, which is better than the commercially available alumina wear resistant material. Hence, this composition has the potential for use as an abrasion resistant material in low impact applications.

The microstructures of the F-0, F-5, F-10, F-15, F-20 and F-25 samples are given in Figs. 5 and 6. The micrographs suggest the following observations:

Table 2
Properties of zirconia-flyash material

Composition	B.D[a] (g/cc)	MOR[b] (MPa)	Hardness[c] *HV* 1.0 (*CV*[f] in %)	MOE[d] (GPa)	AVL[e] (mm^3)
F-0	2.57	57	337 (12.03)	89	13.9
F-5	2.67	73	364 (8.018)	93	9.4
F-10	2.76	126	417 (7.82)	98	8.2
F-15	2.84	117	505 (9.4)	104	2.7
F-20	2.95	109	535 (8.8)	109	3.5
F-25	3.00	89	544 (6.958)	114	3.0

[a] B.D. = bulk density.
[b] MOR = modulus of rupture (3 point bend strength).
[c] Hardness in Vickers scale at 1 kg load.
[d] MOE = modulus of elasticity.
[e] AVL = adjusted abrasion volume loss.
[f] CV = coefficient of variation.

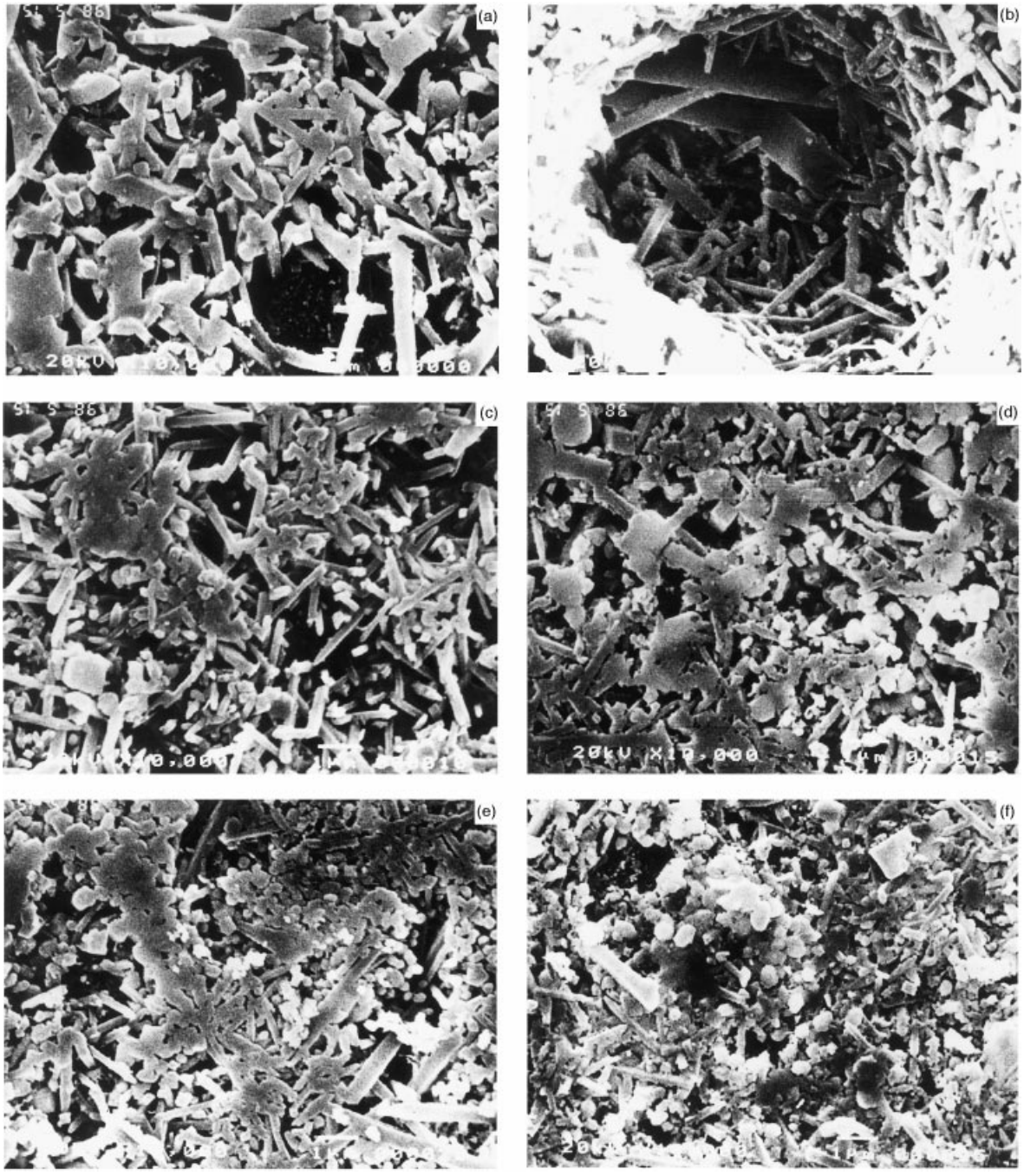

Fig. 5. Scanning electron micrographs of zirconia-flyash material ($\times = 10{,}000$) (a): F-0; (b): F-5; (c): F-10; (d): F-15; (e): F-20; (f): F-25.

(i) The microstructure of flyash and low zirconia containing flyash samples revealed needle like grains. At higher zirconia content in the matrix, the needle like grains were substituted by the homogenous round grains. Metcalfe and Sant [11] had established a direct relationship between the mean grain size of mullite powder compacts and densities. They pointed out that the presence of liquid silicate phase was associated with the development of microstructures having prismatic mullite grains. Kanka and Schneider [12] had confirmed the above facts by indicating that, especially in the later stages of the reaction sintering of silica and alumina ($>1200°C$), liquid phase sintering produces relatively large prismatic mullite crystals embedded in a fine grained matrix. With the heat treatment in longer duration, the reaction sintering produces a stiff skeleton of interlinked elongated mullite crystals. These two observations and the microstructures obtained in this study (Fig. 5) confirmed the liquid phase sintering of the flyash resulting in a skeleton of interlinked elongated

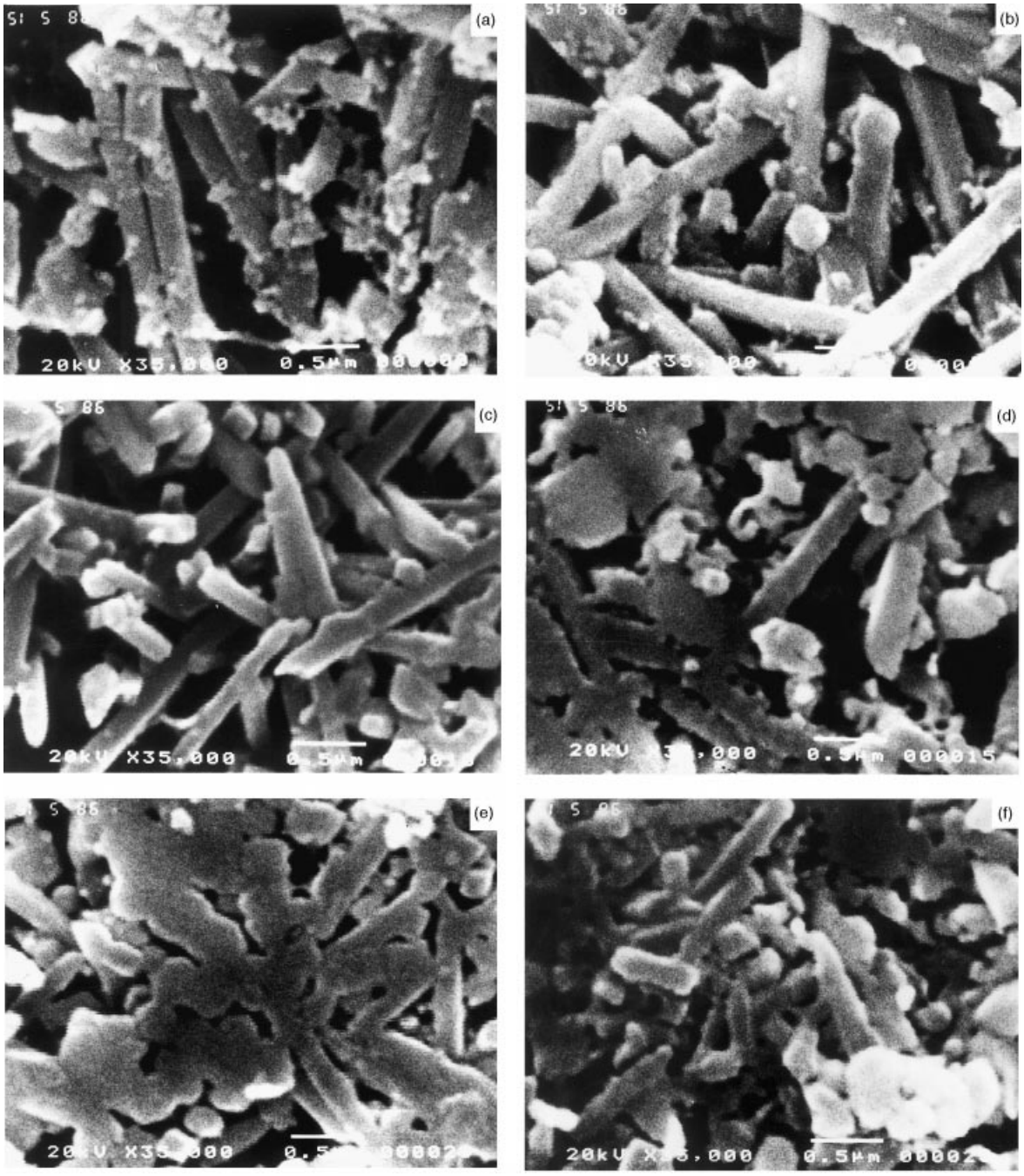

Fig. 6. Scanning electron micrograph of zirconia-flyash material (× = 35,000) (a): F-0; (b): F-5; (c): F-10; (d): F-15; (e): F-20; (f): F-25.

mullite crystals embedded in a fine grained matrix. The origin of the liquid phase at a low temperature is possible due to the presence of alkali ion impurities in the flyash matrix. This fact has been confirmed and published in alumina–silica systems elsewhere [13]. These alkali metal oxide impurities shift the pseudoeutectic point to a lower temperature. This was further confirmed from the binary phase diagrams of constituent compounds [14]. The binary phase diagram of the system Al_2O_3–SiO_2, ZrO_2–Al_2O_3 and ZrO_2–SiO_2 revealed the formation of the liquid phase at a substantially high temperature range of 1550–1850°C, depending on the system. Also, the ternary phase diagram of Al_2O_3–SiO_2–ZrO_2 depicts the formation of liquid phase above 1500°C. However, this work having all the three constituents together were found to sinter at a lower temperature of <1300°C containing a liquid phase. Hence, the origin of the liquid phase have been originated due to the presence of impurities like alkali ion metal oxides and iron oxide, which lower the eutectic temperature of the system. The needle shape of the structures in the present study at low zirconia containing flyash was

found to be substituted by near spherical grains in the microstructure of flyash containing a higher percentage of zirconia in the matrix (Fig. 5). The amount of such grains were found to be increased with the amount of zirconia in the matrix. By comparing the phase structure of these materials [3], the round grains were interpreted as that of the zircon phase and the elongated grains were that of the mullite phase.

(ii) The needle structures were interconnected throughout the material. However, the rounded grains of very uniform size were found to be scattered. The composition controlled microstructural development of these materials directly control the mechanical properties. The interlinked network of prismatic mullite crystals occurring in the F-0–F-10 range of composition, produces favourable mechanical strength values by reinforcement. This may explain the lower bending strength behaviour in F-20 and F-25 compositions due to low interconnection of grains in the structure.

(iii) The size of the needles varied from around 2.5 μm in F-0 composition to around 1.0 μm in F-25 composition. The width of the needle as measured from the high magnification images (Fig. 6) were found to remain constant at a range of 0.2–0.3 μm. The round grain size in the F-20 and F-25 compositions were found to be approximately 0.3 μm. Such a fine grain size of both the needles and the spherical grains and their reinforcement helped in increasing MOR, MOE and hardness values and reducing the abrasion volume loss of the material with increase in ZrO_2 content in the flyash matrix.

(iv) The different size and shape of grains and porosity present in all materials indicates the probability of a variation in hardness, depending on the position of the indenter. Hence, the coefficient of variation of the hardness data varies between 6 and 12%, though lies within the acceptable range.

4. Conclusions

The paper highlights the mechanical properties, abrasion property and the microstructural properties of zirconia-flyash material.

The study reveals the following:

(i) as the ZrO_2 content increased in flyash, more and more Zircon are formed.

(ii) There is an increase in trend in hardness and MOE and MOR upto some extent with increase in ZrO_2 in the flyash matrix.

(iii) The adjusted abrasion volume loss of these materials followed the reduction trend until F-15 composition. The lower AVL value of the F-15 composition can be considered as a potential abrasion resistant material for low impact applications.

(iv) Based on the observation earlier [3] and the data presented here, it is worthwhile to explore the material flyash with 10–15 wt% ZrO_2 for a structural ceramic component in refractory and non-wetting applications.

(v) The present study added a dimension to the application of flyash to produce value added ceramic products like, Zircon. Earlier, there were reports on synthesis of cordierite, glass ceramics, zeolite, ashalloy etc. From flyash.

References

[1] L.N. Satapathy, Wealth from waste, PGDEE thesis, Indian Institute of Ecology and Environment, New Delhi, 1996.
[2] N.N. Sampath Kumar, A.M. Umarji, B.K. Chandrasekhar, Synthesis of α-cordierite (indialite) from flyash, Mat. Res. Bull. 30 (9) (1995) 1107–1114.
[3] L.N. Satapathy, The physical, thermal and phase identification studies of zirconia-flyash material, Ceram. Int. 24 (3) (1998) 199–203.
[4] X. Huang, J.Y. Hwang, B.C. Mutsuddy, Properties of mullite synthesized from flyash and alumina mixture, Interceram 44 (2) (1995) 65–71.
[5] A.R. Boccaccini, M. Petitmermet, E. Wintermantel, Glass-ceramics from a municipal incinerator flyash, Am. Ceram. Soc. Bull. 11 (1997) 75–78.
[6] R. Stevens, An introduction to zirconia, Magnesium Elektron Ltd., UK Publication, 1986.
[7] L.N. Satapathy, Toughened Ceramics, Project report of Ceramic Technological Institute, BHEL, Bangalore, India, 1993.
[8] A.H. Heuer, L.W. Hobbs, Advances in Ceramics, vol.3, Science and Technology of Zirconia, American Ceramic Society, Columbus, OH, 1983.
[9] N. Claussen, M. Ruhle, A.H. Heuer, Advances in Ceramics, vol.12, Science and Technology of Zirconia, American Ceramic Society, Columbus, OH 1983.
[10] D.J. Green, R.H.J. Hannink, M.V. Swain, Zirconia Toughened Alumina in Transformation Toughening of Ceramics, CRC Press, pp. 157–226.
[11] B.L. Metcalfe, J.H. Sant, The synthesis, microstructure and physical properties of high purity mullite, Trans. Br. Ceram. Soc. 74 (1975) 193.
[12] B. Kanka, H. Schneider, Sintering mechanism and microstructural development of coprecipitated mullite, J. Mat. Sci. 29 (5) (1994) 1239.
[13] H. Schneider, K. Okada, J.A. Pask, Mullite and mullite ceramics, John Wiley and Sons, 1994.
[14] R.S. Roth, J.R. Dennis, H.F. McMurdie, Phase Diagram for Ceramists, vol. VI, compiled by National Bureau of Standards, edited and published by the American Ceramic Society Inc., OH, 1987, pp. 144, 155, 188 & 400.
[15] R. Morrell, Handbook of Properties of Technical and Engineering Ceramics Crown copyright, UK, 1985.